Effects of Evapotranspiration on Regional Land Surface Temperature in an Arid Oasis Based on Thermal Remote Sensing

Yujiu Xiong, Shaohua Zhao, Jing Yin, Cheng Li, and Guoyu Qiu

***Abstract*— Evapotranspiration (ET) is crucial to arid and semiarid environments because it substantially affects the energy and water cycles. Based on the estimation of continuous ET from barren or sparsely vegetated areas, this letter investigated how ET affects the regional land surface temperature (LST) in the Shiyanghe river catchment area, a typical inland river catchment in Northwest China. ET was estimated during 2008–2011 using a three-temperature model and MODIS data sets. LST was retrieved from the MODIS product (MOD11A2). Results taken from transects that began in the oasis area and ended in the desert reveal that ET decreased, with the daily average ET in the oasis being approximately 1.4 mm larger than that in the desert. By contrast, the LST in the oasis was 8 K lower than that in the desert. Statistical results suggested that ET and LST showed a negative relationship ($R^2 = 0.83$). Further analysis showed that the correlation was strongly dependent on the water availability in barren or sparsely vegetated areas. It is concluded that in water-limited barren or sparsely vegetated regions, the negative correlation between ET and LST may provide alternative information for water management, such as identifying groundwater recharge in arid regions.**

***Index Terms*— Evapotranspiration (ET), land surface temperature (LST), Moderate Resolution Imaging Spectroradiometer (MODIS), Shiyanghe river catchment, thermal remote sensing, three-temperature model (3T model).**

I. Introduction

EVAPOTRANSPIRATION (ET) includes evaporation from the soil and water surface and vegetation transpiration. ET is significant because it is a key hydrological variable that links the water, energy, and carbon cycles. Therefore, information on the spatial distribution of ET is required in water and energy-related applications.

Remote sensing imagery is becoming an unprecedented source of land surface data that is logistically and economically impossible to be obtained through ground-based observation, and is useful for retrieving surface variables [e.g., land surface temperature (LST)] [1]. These advantages make remote sensing the most feasible technology for monitoring spatiotemporal distributions of ET from regional to global scales [2]–[4].

Although substantial progresses have been made in quantifying spatiotemporal ET [2]–[6], it is still challenging to accurately estimate ET from remote sensing data as land surface is heterogeneous and the ET process involves many controlling factors (e.g., plant biophysics and soil properties) [7]–[9]. In water-limited arid areas, it is even more difficult to estimate ET, especially in barren or sparsely vegetated regions. For example, ET in barren regions was excluded from model calculations in MOD16 [3] and AVHRR ET [4]. However, the annual ET in these barren areas can be relatively high, e.g., exceeding 75 mm/y and accounting for 92%–126% of precipitation [10]. Therefore, lack of accurate information on spatiotemporal ET in barren or sparsely vegetated regions may limit applications of ET products such as MOD16.

In addition, in arid northern China, evaporative fraction, the ratio between latent heat flux and available energy, is reported to be approximately 0.9 in a dense maize land in the growing season, whereas it is 0.3 in a desert steppe [11]. Transpiration of vegetation, therefore, could lead to an evident cooling effect during the growing season [12], [13]. In other arid areas, such as the southern Great Plains [14], California [15], and southern Israel [16], ET increased by irrigation can consequently lead to an LST decrease. However, increased ET may increase soil moisture depletion in water-limited environments leading to the observed increase in LST [17], i.e., LST can be affected by ET in an opposing way. ET in forest was reported to have a warming effect on dry regions, because the ET cooling effect can be constrained due to water availability whereas with lower albedo, forests absorb more shortwave radiation [18]. Thus, the effects of ET on LST remain unclear in arid regions.

The objectives of this letter include: 1) to estimate spatiotemporal ET in barren or sparsely vegetated areas and 2) to investigate the quantitative relationship between LST and ET in an arid oasis.

Manuscript received July 31, 2015; revised April 29, 2015, November 28, 2015, June 11, 2016, and September 5, 2016; accepted October 7, 2016. This work was supported in part by the National Natural Science Foundation of China under Grant 41671416, Grant 41201433, Grant 91025008, and Grant 41101313, in part by the China Scholarship Council under Grant 201606380186, and in part by the Specialized Research Fund for the Doctoral Program of Higher Education of China under Grant 20110171120001. *(Corresponding author: Guoyu Qiu.)*

Y. Xiong is with the Department of Water Resources and Environment, School of Geography and Planning, Sun Yat-sen University, Guangzhou 510275, China, and also with the Department of Land, Air and Water Resources, University of California at Davis, Davis, CA 95616 USA (e-mail: xiongyuj@mail.sysu.edu.cn).

S. Zhao is with the Satellite Environmental Center, Ministry of Environmental Protection, Beijing 100094, China (e-mail: zshyytt@126.com).

J. Yin is with the Institute of Water Resources and Hydropower Research, Beijing 100038, China (e-mail: yinjing@iwhr.com).

C. Li and G. Qiu are with the Shenzhen Engineering Laboratory for Water Desalinization with Renewable Energy, School of Environment and Energy, Peking University, Shenzhen 518055, China (e-mail: qiugy@pkusz.edu.cn; licheng520.1001@163.com).

Color versions of one or more of the figures in this letter are available online at http://ieeexplore.ieee.org.

Digital Object Identifier 10.1109/LGRS.2016.2616409

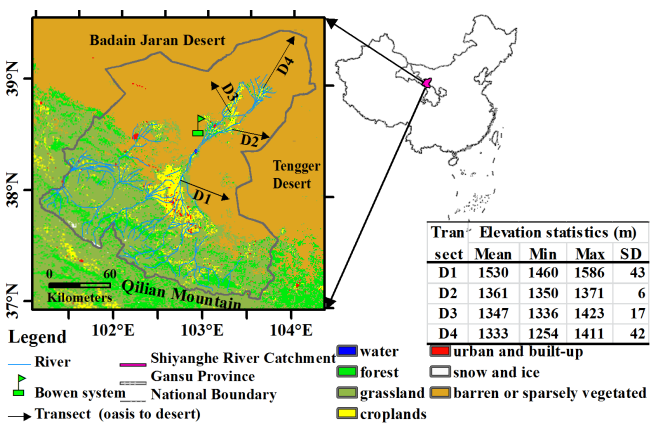

Transect	Elevation statistics (m)			
	Mean	Min	Max	SD
D1	1530	1460	1586	43
D2	1361	1350	1371	6
D3	1347	1336	1423	17
D4	1333	1254	1411	42

Fig. 1. Location of the study area and land use and land cover map based on MODIS land use product (MCD12Q1) with the International Geosphere-Biosphere Programme classification scheme. Note: forests include evergreen needleleaf/broadleaf forests, deciduous needleleaf/broadleaf forests, mixed forests, and open and closed shrublands. Grasslands include grasslands, savannas, and woody savannas. The elevation statistics is based on the Shuttle Radar Topography Mission 90 m DEM.

II. Data and Methodology

A. Description of the Study Area

The study area in the Shiyanghe river catchment covers about 40 579 km^2, and is located at approximately 36° 29′ −39° 27′ N and 101° 41′ −104° 16′ E on the northern slope of Qilian Mountain and the eastern part of the Hexi Corridor in Gansu province, Northwest China (Fig. 1). The Shiyanghe River is an inland river that originates in the southern part of the Qilian Mountain and ends at the Minqin Oasis. Most of the area is flat (elevation 1300–2000 m) except for the Qilian Mountain highland area in the south (elevation 2000–5500 m). The climate changes from south to north: the south is a cold semiarid to semihumid area with an annual precipitation of 300–600 mm and pan evaporation of 700–1200 mm; the middle is the Hexi Corridor, a cool and arid area with an annual precipitation of 150–300 mm and pan evaporation of 1200–2000 mm; the north land, surrounded by the Badain Jaran and Tengger deserts, is temperate arid with an annual precipitation of less than 150 mm and pan evaporation of more than 2000 mm [19]. Due to limited water resources, the area has suffered a serious loss of natural vegetation, gradual soil salinization, and desertification [19], [20].

B. Data Preparation

The data sets used for this letter include an 8-day MODIS LST/emissivity data (MOD11A2) at 1 km spatial resolution and an ET product at 1 km spatial resolution and 16-day temporal resolution estimated using a three-temperature model (3T model) and MODIS data. All of the MOD11A2 (version 5) were recorded between 2008 and 2011 and provided free of cost by NASA. The 3T model, based on energy balance without requiring aerodynamic resistance, has been tested to be simple and accurate [10], [21]–[26]

$$E_s = \frac{1}{L}\left(R_{n,s} - G_s - (R_{n,\mathrm{sr}} - G_{\mathrm{sr}})\frac{T_s - T_a}{T_{\mathrm{sr}} - T_a}\right) \quad \text{soil evaporation} \tag{1}$$

$$E_c = \frac{1}{L}\left(R_{n,c} - R_{n,\mathrm{cr}}\frac{T_c - T_a}{T_{\mathrm{cr}} - T_a}\right) \quad \text{vegetation transpiration} \tag{2}$$

$$\mathrm{ET} = E_s + E_c \quad \text{evapotranspiration} \tag{3}$$

where ET is evapotranspiration, and E_s and E_c are the soil and vegetation components of ET, respectively, both in millimeters; L is the latent heat of vaporization; the subscripts "s," "c," "a," "sr," and "cr" represent soil, canopy, atmosphere, reference soil, and reference canopy, respectively; R_n is net radiation and G is soil heat flux, both in W/m^2; T is temperature in K.

In this letter, soil surface temperature (T_s) and canopy temperature (T_c) were calculated using LST (MOD11A2) and the normalized difference vegetation index (MOD13A2) by assuming that LST is a weighted summation of T_s and T_c [27]. T_a, the mean daily value for every 16-day period according to the composition dates of the MODIS product (MOD13A2) was calculated from the daily air temperature of Minqin national meteorological station. T_{sr} and T_{cr} for each period were the maximum value for the T_s and T_c, respectively [25]–[26], obtained from the decomposed MOD11A2 over the study area. R_n and G were retrieved from MODIS products (version 5), and detailed descriptions of the model parameterization can be found in [24]–[26]. The instantaneous ET estimated from the 3T model was extrapolated to daily value (a mean value for a 16-day period) based on a sinusoidal function for cloudless days (4) according to [28]; details about the equation are available in [25]. Then, the daily ETs were scaled to 16-day (or yearly) values by considering a cloud coefficient [29]. The cloud coefficient was equal to 0.65 and was calculated using the meteorological data: mean annual cloud cover and the number of sunny days for the period from 1981 to 2010

$$\mathrm{ET}_D = \mathrm{ET}\frac{2N}{\pi \sin(\pi \cdot t/N)} \tag{4}$$

where ET and ET_D are the instantaneous and daily (here a mean value for a 16-day period) ET rates, respectively. N is the duration of ET during the daytime and t is the time between sunrise and the data collection time of the passing satellite sensor.

Four transects (lines D1, D2, D3, and D4 in Fig. 1), beginning at the oasis and ending in the desert, were selected so that the changes in LST and ET could be measured. Lines D1, D2, and D3 were almost perpendicular to the main stream, whereas line D4 was an extension of the main stream.

C. Method to Evaluate ET Estimation

ET estimation was compared with flux tower ET and water balance ET. Flux tower ET was calculated from a Bowen ratio system installed at a sparsely vegetated desert around Minqin oasis (102° 55′ 5″ E, 38° 37′ 48″ N), operating from May 2010 to December 2011 [10]. Observational items include soil heat flux at 2 and 5 cm, respectively, below the ground surface, air temperature and relative humidity over ground at two different heights (i.e., 1.5 and 2.0 m), and other routine meteorological factors (e.g., net radiation) over ground at a 2 m height. All data were collected by a datalogger (model DT500 series 3, Datataker, Australia) at every 5 s.

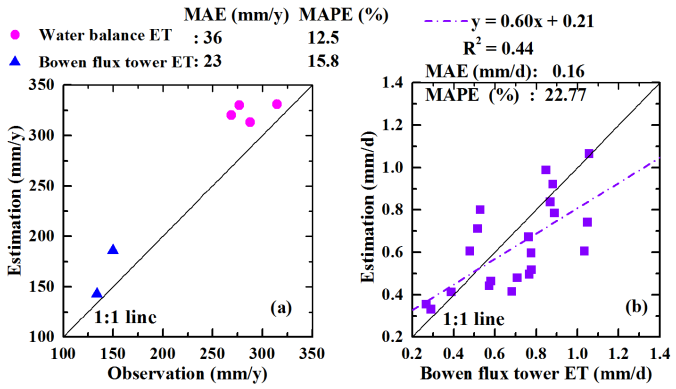

Fig. 2. Comparison of the estimated and observed ET. (a) Yearly scale. (b) Daily scale. MAE and MAPE represent mean absolute error and mean absolute percent error, respectively.

The daily ET was the sum of instantaneous values (i.e., mean value of each 10 min) through the Bowen ratio energy balance method. Water balance ET from 2008 to 2011 was used to assess the modeled ET. Generally, the water balance equation for a river basin at a yearly scale can be written as [30]

$$\mathrm{ET_{WBE}} = P - R - \triangle S \tag{5}$$

where P, R, ΔS, and $\mathrm{ET_{WBE}}$ are precipitation, runoff, water storage change, and ET in millimeters, respectively. An endorheic basin has no runoff at basin outlet ($R = 0$). In the study basin, irrigation (I) consumes approximately 86% of the total water use [20], thus it was taken into account. When water storage change is assumed to be zero [31], (5) can be simplified to (6). All of the precipitation (calculated using Thiessen polygon method) and irrigation data were provided by the water resources bulletin of Gansu province

$$\mathrm{ET_{WBE}} = P + I. \tag{6}$$

The mean absolute error (MAE) and mean absolute percent error (MAPE) were used to assess the difference between the model estimation and observation [25].

III. Results and Discussion

A. Assessment of the Estimated ET

Fig. 2 shows a comparison between the estimated ET and water balance ET as well as the Bowen ratio flux tower ET as follows.

1) At yearly scale, the differences between the estimated ET and Bowen ratio flux tower ET are small, with margins of 9 and 36 mm for 2010 and 2011, respectively.
2) At the basin scale, the MAE (MAPE) between the estimated ET and water balance ET is 36 mm/y (12.5%) over the four years, with values of 25, 53, 51, and 16 mm/y in 2008–2011, respectively.
3) At daily scale, the MAE and MAPE are 0.16 mm d^{-1} and 22.77%, respectively, for the sparsely vegetated sandy desert. The errors indicate that biases exist in the ET estimations. The bias may be caused by uncertainties in observations and model parameterizations [26]. For instance, ET_{WBE} is likely underestimated, because the precipitation records do not include snowfall and illegal groundwater mining used for irrigation cannot be monitored and quantified. Additionally, the cloud coefficient may cause uncertainty when scaling daily ET to periodical values (here 16-day). The coefficient should be calculated using the observed cloud cover and the number of sunny days for each 16-day interval [29]. However, in this letter the cloud coefficient is a mean annual value owing to the lack of meteorological observations. This assumption may lead to estimation uncertainty. For example, if the cloud coefficient has an uncertainty of ±10% and increases to 0.715 in 2008, the ET will increase by 32 mm. Nevertheless, the comparison indicated that the estimated ET was close to the observed ET.

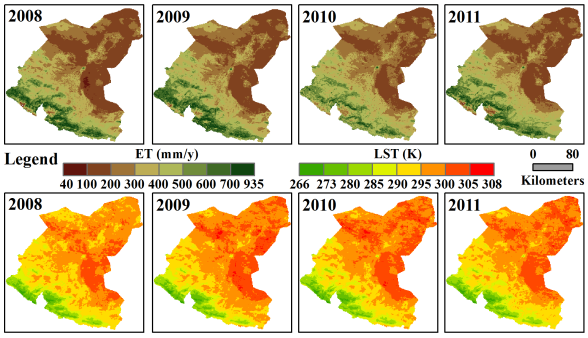

Fig. 3. Annual ET and LST maps of Shiyanghe river catchment. Top: maps are the annual ET for 2008–2011, respectively. Bottom: maps are the annual LSTs.

B. Spatial Characteristics of ET and LST

Fig. 3 shows that ET decreases gradually from south to north, whereas LST increases. For example, ET declines along a gradient starting in the southern mountain areas (>400 mm/y) with abundant vegetation coverage, and moving down into the sparsely vegetated regions in the north (<100 mm/y). This change in trend is in good accordance with the regional climate and vegetation distribution. The southern part of the study area belongs to semiarid climate while the northern part belongs to arid, and thus the precipitation in the north is lower than that in the south, leading to a higher ET in the south.

C. ET Effects on Land Surface Temperature

The effects of ET on LST were investigated in two ways using the data collected from transects that began inside the oasis and moved toward the desert area, and from different land cover types (desert and oasis).

Fig. 4 shows that ET declines and LST increases from inside the oasis toward the desert. LST increases quickly within the first 10 km (from about 304–312 K) and then shows little change thereafter. According to the 90 m digital elevation model (DEM) [32], the topographic gradient of each transect is very small, with a maximum standard deviation of 43 m (table in Fig. 1). The statistics indicate that the topographic gradient may have little impact on the LST change. However, ET decreases within the first 10 km, located in the oasis with

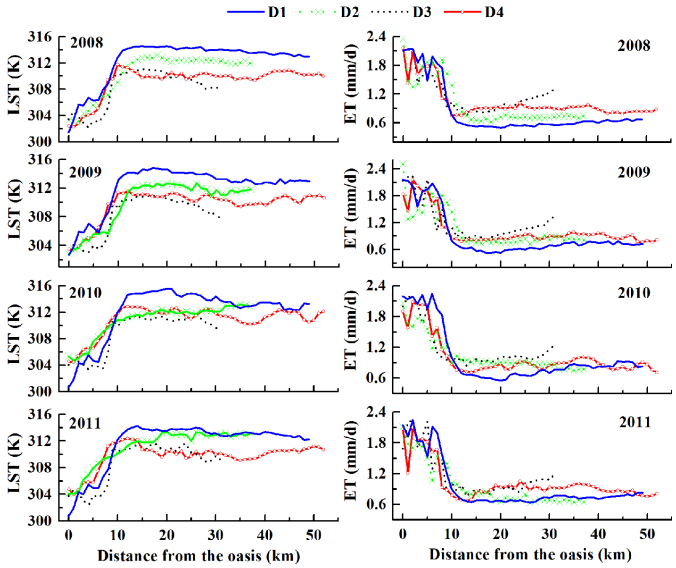

Fig. 4. Value of LST and ET versus distance (km) inside oasis toward desert in the growing season. Note: D_i represents the observational line i ($i = 1, 2, 3, 4$), see Fig. 1 for details. LST is the mean value of MOD11A2 between DOY 161 and 289 in each year, and ET is the mean value of ET in the corresponding period.

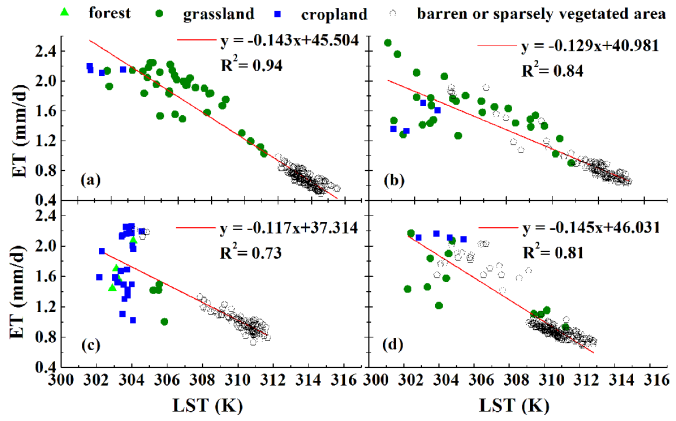

Fig. 5. Scatterplots showing the relation between LST and ET of the transects based on Fig. 4, for lines (a) D1, (b) D2, (c) D3, and (d) D4.

good water conditions and vegetation cover, from approximately 2.2 to 0.8 mm/d, and then changes little thereafter (Fig. 4). In the desert areas, the LST is about 8–12 K larger than that in the oasis area. A daily ET of 1.0–2.0 mm/d could reduce the LST by 8–12 K. This is because in the vegetated area ET consumes approximately 39% of net radiation on average, whereas in barren or sparsely vegetated areas it only consumes a maximum of 30% of net radiation. Statistical results further suggested that although LST was obtained at the moment of MODIS overpass (approximately around 12:00 local time), ET and LST are negatively correlated, with determination coefficients (R^2) (slope in mm/d/K) of 0.94 (−0.143), 0.84 (−0.129), 0.73 (−0.117), and 0.81 (−0.145), respectively, for D1, D2, D3, and D4 (Fig. 5). These results indicate that the ET from oasis has a statistically significant cooling effect in the inland river catchment area.

Fig. 6 shows the relation between mean annual ET and LST of different land use types. The barren or sparsely vegetated area accounts for 50.49% of the study region, and the

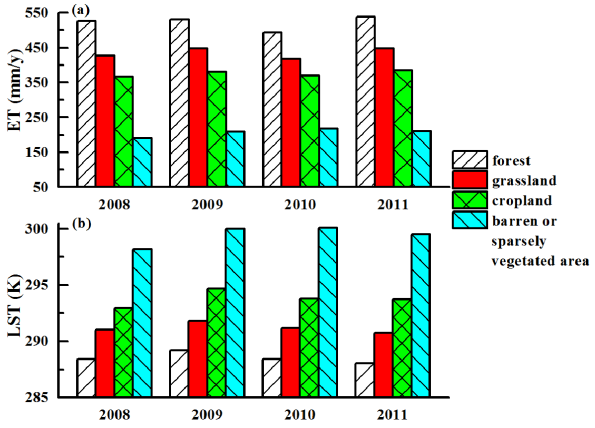

Fig. 6. Mean annual ET (a) and LST (b) of different land cover/use types .

remaining includes grassland, forest, and cropland with ratios of 34.08%, 9.01%, and 5.12%, respectively. Forests correspond to the highest ET, undulating around 500 mm for the four years. The ET of grassland (around 420 mm) is higher than that of cropland (around 380 mm). Although having the largest area, barren or sparsely vegetated lands have the lowest ET, with a value of around 200 mm. Meanwhile, LST of desert is the highest. Statistics based on Fig. 6 show that at yearly scale, the linear relationship between ET and LST is significant, with R^2 (slope in mm/y/K) of 0.96 (−27.805). The results shown in Figs. 5 and 6 indicate that ET and LST in the arid region generally showed a negative relationship.

In this letter, ET estimation is dependent on LST, and a correlation between the LST and ET values may be implicit. However, statistics using MOD16 (an ET product estimated based on the Penman–Monteith method without using LST) and MOD11A2 in vegetated areas of the four transects indicate that LST and ET also showed a negative relation, with a mean R^2 (slope in mm/d/K) of 0.70 (−0.09). The results indicate that the relation between LST and ET obtained in this letter is reliable.

However, the relation between ET and LST may be more complicated than the results shown here, especially in arid regions characterized as high moisture constraint and low, nonuniform vegetation cover. In this letter, the negative correlation between ET and LST was strongly dependent on data obtained from barren or sparsely vegetated area, because most points from these regions distributed closely along the regression line, especially when LST was larger than 308 K or when ET values were lower than 1.2 mm/d (black pentagons in Fig. 5). For the other land use type, the negative correlation was poor, and a positive correlation was observed between limited ET and LST values of forest [green triangles in Fig. 5(c)], with R^2 (slope in mm/d/K) of 0.92 (0.50). This may be a result of the two major factors (i.e., energy and water) that control ET. Soil water availability in oasis is better than in desert; therefore, ET from vegetated areas in the oasis is strongly controlled by both radiation and soil water, and ET values for a given land type may show certain differences due to variation in the soil water availability. In contrast, ET from barren or sparsely vegetated areas is controlled only by soil water, and water limitation leads to a significant negative relationship between ET and LST.

IV. Conclusion

Based on the estimation of spatiotemporal ET in barren or sparsely vegetated areas, the quantitative relationships between ET and regional LST was investigated in a typical arid inland-river basin in Northwest China. Statistical results suggest that ET decreases along transects beginning inside the oasis and moving toward the desert area, with the average daily ET in the oasis being approximately 1.4 mm larger than that in the desert area. In contrast, LST in the oasis is 8 K lower than that in the desert. Further analysis showed a negative relationship between ET and LST, with a mean determination coefficient (R^2) of 0.83, and the significant correlation was strongly dependent on the water availability in barren or sparsely vegetated areas. The relation between ET and LST may provide alternative information for water management, such as identifying groundwater recharge in arid regions.

The estimated ET will be thoroughly tested in combination with more flux tower data, and the feedback mechanism behind ET and temperature in arid region warrant further study.

Acknowledgment

The authors would like to thank the China Meteorological Administration for providing meteorological data, to the NASA Land Processes Distributed Active Archive Center for providing MODIS products, to L. Priscilla and Dr. S. H. Du from Peking University for improving the writing quality, and to the anonymous reviewers for their constructive comments.

References

[1] F. Becker and Z. L. Li, "Towards a local split window method over land surface temperature from a satellite," *Int. J. Remote Sens.*, vol. 11, no. 3, pp. 369–394, May 1990.

[2] W. G. M. Bastiaanssen, M. Menenti, R. A. Feddes, and A. A. M. Holtslag, "A remote sensing surface energy balance algorithm for land (SEBAL). 1. Formulation," *J. Hydrol.*, vols. 212–213, pp. 198–212, Dec. 1998.

[3] Q. Mu, M. Zhao, and S. W. Running, "Improvements to a modis global terrestrial evapotranspiration algorithm," *Remote Sens. Environ.*, vol. 115, no. 8, pp. 1781–1800, Aug. 2011.

[4] K. Zhang, J. S. Kimball, R. R. Nemani, and S. W. Running, "A continuous satellite-derived global record of land surface evapotranspiration from 1983 to 2006," *Water Resour. Res.*, vol. 46, no. 9, p. W09522, Sep. 2010, doi:10.1029/2009WR008800.

[5] R. G. Allen, M. Tasumi, and R. Trezza, "Satellite-based energy balance for mapping evapotranspiration with internalized calibration (METRIC)—Model," *J. Irrigation Drainage Eng.*, vol. 133, no. 4, pp. 395–406, Aug. 2007.

[6] J. M. Norman, W. P. Kustas, and K. S. Humes, "Source approach for estimating soil and vegetation energy fluxes in observations of directional radiometric surface temperature," *Agricult. Forest Meteorol.*, vol. 77, nos. 3–4, pp. 263–293, Mar. 1995.

[7] Y. T. Yang, D. Long, and S. H. Song, "Remote estimation of terrestrial evapotranspiration without using meteorological data," *Geophys. Res. Let.*, vol. 40, no. 12, pp. 3026–3030, Jul. 2013.

[8] Z. L. Li *et al.*, "A review of current methodologies for regional evapotranspiration estimation from remotely sensed data," *Sensors*, vol. 9, no. 5, pp. 3801–3853, May 2009.

[9] D. Long, L. Longuevergne, and B. R. Scanlon, "Uncertainty in evapotranspiration from land surface modeling, remote sensing, and GRACE satellites," *Water Resour. Res.*, vol. 50, pp. 1131–1151, Feb. 2014.

[10] G. Y. Qiu, C. Li, and C. H. Yan, "Characteristics of soil evaporation, plant transpiration and water budget of *Nitraria* dune in the arid northwest China," *Agricult. Forest Meteorol.*, vol. 203, pp. 107–117, Jan. 2015.

[11] T. Xu, S. M. Bateni, and S. Liang, "Estimating turbulent heat fluxes with a weak-constraint data assimilation scheme: A case study (HiWATER-MUSOEXE)," *IEEE Geosci. Remote Sens. Lett.*, vol. 12, no. 1, pp. 68–72, Jan. 2015.

[12] L. Bounoua *et al.*, "Sensitivity of climate to changes in NDVI," *J. Climate*, vol. 13, no. 13, pp. 2277–2292, Jul. 2000.

[13] D. Sun and R. Pinker, "Factors contributing to the spatial variability of satellite estimates of diurnal temperature range in the United States," *IEEE Geosci. Remote Sens. Lett.*, vol. 11, no. 9, pp. 1524–1528, Sep. 2014.

[14] J. Ge, "MODIS observed impacts of intensive agriculture on surface temperature in the southern Great Plains," *Int. J. Climatol.*, vol. 30, no. 13, pp. 1994–2003, Nov. 2010.

[15] G. Leng, M. Huang, Q. Tang, W. J. Sacks, H. Lei, and L. R. Leung, "Modeling the effects of irrigation on land surface fluxes and states over the conterminous United States: Sensitivity to input data and model parameters," *J. Geophys. Res. Atmos.*, vol. 118, no. 17, pp. 9789–9803, Sep. 2013.

[16] K. De Ridder and H. Gallée, "Land surface–induced regional climate change in Southern Israel," *J. Appl. Meteorol.*, vol. 37, no. 11, pp. 1470–1485, Nov. 1998.

[17] J. Peñuelas, T. Rutishauser, and I. Filella, "Phenology feedbacks on climate change," *Science*, vol. 324, no. 5929, pp. 887–888, May 2009.

[18] Y. Li, M. S. Zhao, S. Motesharrei, Q. Z. Mu, E. Kalnay, and S. C. Li, "Local cooling and warming effects of forests based on satellite observations," *Nature Commun.*, vol. 6, p. 6603, Mar. 2015.

[19] Z. Ma, S. Kang, L. Zhang, L. Tong, and X. Su, "Analysis of impacts of climate variability and human activity on streamflow for a river basin in arid region of northwest China," *J. Hydrol.*, vol. 352, nos. 3–4, pp. 239–249, May 2008.

[20] G. Geng and R. Wardlaw, "Application of multi-criterion decision making analysis to integrated water resources management," *Water Resour. Manag.*, vol. 27, pp. 3191–3207, Apr. 2013.

[21] G. Y. Qiu, T. Yano, and K. Momii, "An improved methodology to measure evaporation from bare soil based on comparison of surface temperature with a dry soil surface," *J. Hydrol.*, vol. 210, nos. 1–4, pp. 93–105, Sep. 1998.

[22] G. Y. Qiu, K. Miyamoto, S. Sase, Y. Gao, P. Shi, and T. Yano, "Comparison of the three-temperature model and conventional models for estimating transpiration," *Jpn. Agricult. Res. Q.*, vol. 36, no. 2, pp. 73–82, 2002.

[23] G. Y. Qiu, P. Shi, and L. Wang, "Theoretical analysis of a remotely measurable soil evaporation transfer coefficient," *Remote Sens. Environ.*, vol. 101, no. 3, pp. 390–398, 2006.

[24] Y. J. Xiong and G. Y. Qiu, "Estimation of evapotranspiration using remotely sensed land surface temperature and the revised three-temperature model," *Int. J. Remote Sens.*, vol. 32, no. 20, pp. 5853–5874, Oct. 2011.

[25] Y. J. Xiong and G. Y. Qiu, "Simplifying the revised three-temperature model for remotely estimating regional evapotranspiration and its application to a semi-arid steppe," *Int. J. Remote Sens.*, vol. 35, no. 6, pp. 2003–2027, Mar. 2014.

[26] Y. J. Xiong, S. H. Zhao, F. Tian, and G. Y. Qiu, "An evapotranspiration product for arid regions based on the three-temperature model and thermal remote sensing," *J. Hydrol.*, vol. 530, pp. 392–404, Nov. 2015.

[27] J.-P. Lhomme, B. Monteny, and M. Amadou, "Estimating sensible heat flux from radiometric temperature over sparse millet," *Agricult. Forest Meteorol.*, vol. 68, nos. 1–2, pp. 77–91, Mar. 1994.

[28] R. D. Jackson, J. L. Hatfield, R. J. Reginato, S. B. Idso, and P. J. Pinter, Jr., "Estimation of daily evapotranspiration from one time-of-day measurements," *Agricult. Water Manage.*, vol. 7, nos. 1–3, pp. 351–362, 1983.

[29] Y. J. Xiong, G. Y. Qiu, S. H. Zhao, and F. Tian, "Estimating regional evapotranspiration using a three-temperature model and MODIS products," in *Remote Sensing of the Terrestrial Water Cycle*, V. Lakshmi, Ed., 1st ed. Hoboken, NJ, USA: Wiley, 2014, pp. 83–94.

[30] Y. F. Shi *et al.*, "Recent and future climate change in northwest China," *Climatic Change*, vol. 80, no. 3, pp. 379–393, Aug. 2007.

[31] B. Z. Zhang, S. Z. Kang, F. S. Li, and L. Zhang, "Comparison of three evapotranspiration models to Bowen ratio-energy balance method for a vineyard in an arid desert region of northwest China," *Agricult. Forest Meteorol.*, vol. 148, no. 10, pp. 1629–1640, Sep. 2008.

[32] A. Jarvis, H. I. Reuter, A. Nelson, and E. Guevara. (2008). *Hole-Filled Seamless SRTM Data V4*, International Centre for Tropical Agriculture (CIAT), accessed on Jul. 6, 2016. [Online]. Available: http://srtm.csi.cgiar.org